Materials Research Proceedings **2** (2016) 139-144 doi: http://dx.doi.org/10.21741/9781945291173-24

Cementite Residual Stress Analysis in Gas-nitrided Low Alloy Steels

L. Barrallier[1,a*], S. Goekjian[1,b], F. Guittonneau[1,c], S. Jégou[1,d]

[1] MSMP Laboratory, Arts et Métiers ParisTech, 2 cours des Arts et Métiers, F-13617 Aix-en-Provence, France

[a] laurent.barrallier@ensam.eu, [b] sarah.goekjian@ensam.eu, [c] fabrice.guittonneau@ensam.eu, [d] sebastien.jegou@ensam.eu

Keywords: Nitriding, Residual Stress, X-ray Diffraction, EBSD

Abstract. This paper deals with the measurement of residual stresses in cementite after gas-nitriding of a 33CrMoV12-9 steel. During nitriding, precipitation of nanometric alloying elements nitrides and cementite at grain boundaries occurs leading to an increase of superficial hardness and providing compressive residual stresses in the surface layer. The stress state in the ferritic matrix has generally been measured to characterize the mechanical behaviour of the nitrided case while the other phases are not taken into account. In order to better understand the mechanical behaviour (e.g. fatigue life and localization of cracks initiation) of heterogeneous material such as in case of nitrided surfaces, the nature (sign, level) of residual stresses (or pseudo-macro-stresses) of the present phases can be calculated from measurements using X-ray diffraction to select the considered phase. Due to a low volume fraction of cementite through a nitrided case, an approach based on X-ray and electron backscattered diffractions (XRD and EBSD respectively) is proposed to perform stress measurements in cementite. An optimization of the surface preparation (by mechanical and/or chemical polishing techniques) prior to EBSD analysis was performed in order to minimize deformation induced by surface preparation. Pseudo-macro-stresses were calculated in tempered martensite and cementite. Results are compared to local residual stress measurements carried out by a cross-correlation method using EBSD patterns.

Introduction

Gaseous nitriding is a thermochemical surface treatment used to improve surface hardness and generate compressive residual stresses in mechanical steel parts for aeronautics or high performance automotive gearboxes [1]. It involves the diffusion of nitrogen from the surface to the core of the material using an ammonia and nitrogen and/or hydrogen gas mixture. The present work deals with low carbon alloyed steels characterized by a tempered martensite microstructure ($(Cr,Fe)_{23}C_6$/$(Cr,Fe)_7C_3$ carbides in ferrite). The temperature of gaseous nitriding (between 480-580 °C) is chosen below the eutectoid transformation and tempering temperatures (ferrite to austenite in Fe-N binary system) in order to prevent the core material from mechanical properties alterations, but high enough to activate the diffusion of nitrogen [2]. Co-diffusion of carbon occurs during nitriding and contributes to a complex microstructure gradient characterized by tempered carbides transformed into chromium incoherent nitrides (Cr,Mo)N and grain boundary cementite $(Fe,Mo)_3C$. Semi-coherent chromium nitrides also form from the solid solution of chromium into ferrite [3]. Nano-scale (Cr,Mo)N precipitates provide the hardness increase after nitriding [4]. Close to the surface, iron nitrides (γ'-Fe_4N_{1-x}, ε-$Fe_{2-3}N$) generally develop as a compound layer depending on the nitrogen potential [5]. Fig. 1 shows a typical nitriding layer of a 33CrMoV12-9 steel nitrided at 520 °C during 100 h. Precipitation and transformation of phases also generate specific volume changes (in regard to the density of the initial and formed phases) in the nitriding layer leading to the generation of compressive residual stresses at the nitriding temperature and during cooling [3, 6] [7]. Only residual stresses in ferrite have usually been determined using X-ray diffraction technics. A few papers give

Materials Research Proceedings **2** (2016) 133-144 doi: http://dx.doi.org/10.21741/9781945291173-24

the macroscopic stress state using mechanical methods (hole drilling…) [6],8,9]. Due to the multiphase character of nitriding layers, residual stresses depend on the considered crystalline phase (pseudo-macro-stresses) and are different to macro-stresses. The residual stress state is a substantial input for the fatigue resistance of nitrided parts, especially in the case of the initiation of high cycle fatigue (HCF) cracks [10]. Whereas macro-stresses drive the crack propagation, micro-stresses govern the local damage due to heterogeneities at the microstructure scale. The aim of this paper is the determination of residual stresses in the grain boundary cementite in order to take them into account in HCF criteria.

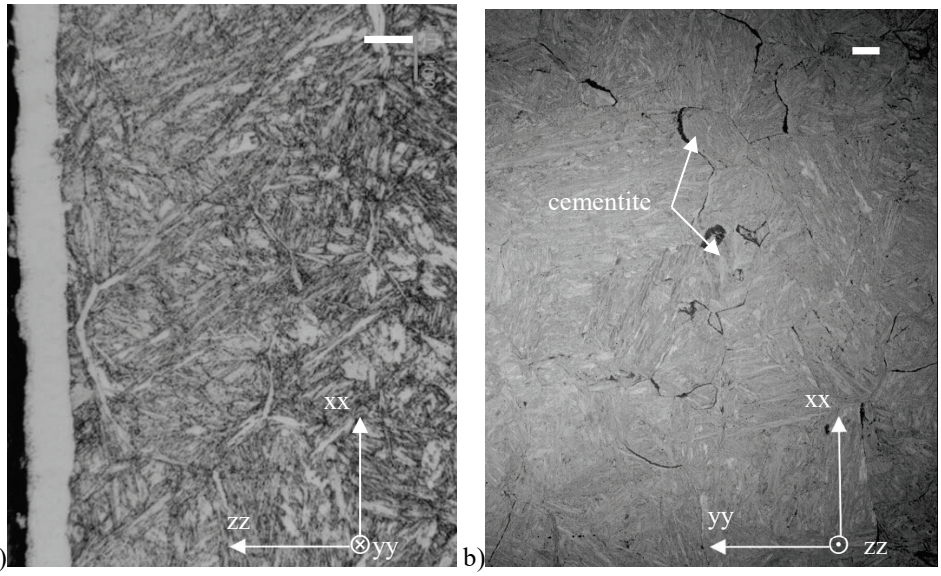

Fig. 1: Nitrided 33CrMoV12-9 @ 520 °C/100 h: a) cross-section optical micrograph showing compound and diffusion layers, b) scanning electron micrograph (SEM) @ 50 µm depth and parallel to the nitrided surface: grain boundary cementite.

Diffraction stress analysis

X-Ray diffraction. Stress analysis can be carried out by X-ray diffraction using crystalline planes as a strain gauge. The $\sin^2\psi$ method is usually chosen in case of polycrystalline and multiphase materials. $\sigma_{xx}^{\phi_i} - \sigma_{zz}^{\phi_i}$ residual stress are only accessible in case of a multiphase (phases ϕ_i) material without unstressed reference (axis are defined in Fig. 1). X-ray elastic constants (XEC) of considered phases must be determined from elastic constants of a single crystal and the orientation distribution function (ODF) of polycrystalline aggregates in case of textured sample. Fig. 2 gives the evolution of the Young modulus $E_{\{hkl\}}$ of Fe_3C orthorhombic single crystal in spherical coordinates (data from [11]). The elastic anisotropy of Fe_3C cementite is highly marked, $E_{\{011\}} = 319$ GPa and $E_{\{110\}} = 65$ GPa. XEC are calculated using homogenization methods based on direct Kröner-Eshelby approach for un-textured materials and polycrystalline Kröner-Eshelby approach using ODF for textured materials.

Electron back scattering diffraction. EBSD was used to determine crystal orientations using SEM electron diffraction pattern (Kikuchi pattern). The gage volume is given by the operating conditions such as the voltage, tilt angle… and nature of the material (electron absorption effect). Orientation maps can be performed at the scale of the microstructure with a 0.1-1 µm spatial resolution. Quantitative stress analysis is based on the measurement of the misorientation of Kikuchi bands. Maurice and al. developed a method using 3D Hough transform [12] while Wilkinson and al. compared Kikuchi patterns with a reference taken from an identical crystal orientation [13]. Based on a cross-correlation method, these technics allow to determine tensorial residual stress maps (assuming σ_zz^(ϕ_i)=0) for a given phase and orientation. For more details see [14,15]. Only the

Materials Research Proceedings **2** (2016) 133-144 doi: http://dx.doi.org/10.21741/9781945291173-24

single crystal elastic constants of the considered phase are needed to perform stress analysis. Such stress mapping actually gives the stress gradient through a single crystal (or grain) and not the absolute residual stresses. It implies that stresses between grains cannot be evaluated.

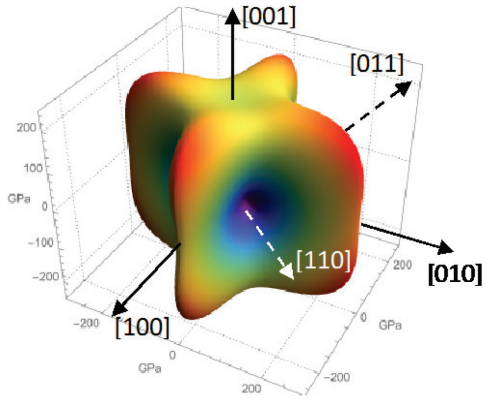

Fig. 2: Young modulus of Fe_3C single crystal (data from [11]).

Experiments

Material. Sample (15×15×6 mm^3) was made from oil quenched (austenitization @ 920 °C/1 h) and tempered (2 h @ 620 °C) 33CrMoV12-9 steel. Gas nitriding was performed at 520 °C during 30 h and $K_N = 4.3$ $atm^{-½}$. The preparation of the sample for stress analyses consists in cutting the sample parallel to the surface at a 50 µm depth. The obtained surface was mechanically polished (220, 500, 1200, 2000, 4000 mesh SiC paper and 1 µm diamond solution), and several finishing preparations (vibrating, ionic and electrolytic polishing) were explored in order to reduce surface plastic deformation and thus optimize the acquisition of Kikuchi patterns.

Surface finishing preparations. Vibrating polishing was performed using a Buehler® VibroMet 2 vibratory device during 16 h with a polishing solution made with 50 mL of colloidal alumina OP AN 0.05 and 200 mL of L PS4 lubricant followed by utrasonic cleaning of the sample during 30 min in pure ethanol. Ionic polishing was performed on a 2×15×6 mm^3 sample using a JEOL® IB-09010CP cross-section polisher operating at 4.5 kV with argon flux during 20 h. Electropolishing was performed on a Struers® Electropol device operating at 15 V and 0.5 A using a Struers A2 electrolyte during 30 s.

Tab. 1: X-ray diffraction parameters used for residual stress and texture analyses.

	Phase	**Texture analysis**	**Stress analysis**	
Device	Seifert®			Siemens®
Mount type	Bragg-	4 circles	χ	Ω
Phase	-	Fe_3C	Fe_3C	α-Fe
Diffracting peak	-	{121}/{210}	{051}	{211}
Wavelength	Cr-Kα			
Voltage [kV]/intensity	40/30			
2θ step [°2θ]	0.03	0.1	0.05	0.032
Time / peak [s]	2000	200	7200	300
Angles [°]	38-141 °2θ	α (0-40°) and β (0-360°) with	9 ψ	13 ψ

Observation and EBSD acquisition. Light micrographs were obtained using a Leica® Aristomet device coupled with a Nikon® digital acquisition system. Surface was etched with a 10 % Nital solution. SEM observations were carried out on a JEOL® 7001F device operating at 15 kV using backscattered electrons. For EBSD analysis, sample was tilted at 70° using hkl® device. Basic EBSD analysis and stress analysis (cross correlation method) were performed using Channel 5 and CrossCourt® softwares respectively.

Materials Research Proceedings **2** (2016) 133-144 doi: http://dx.doi.org/10.21741/9781945291173-24

X-ray diffraction. Residual stress and texture analyses of cementite were performed on Seifert® XRD 3003 PTS and Siemens® D500 devices using position sensitive detector (PSD). Acquisition parameters are given in Tab. 1. Fig. 3 gives the X-ray diffraction spectrum of the analysed surface. The volume fraction of cementite was estimated to 4.6 ± 0.66 % from Rietveld analysis and Maud software [16].

Results

Surface preparation. Several quality parameters were considered to select the best surface finishing preparation. The IR criterion gives the indexing rate of Kikuchi patterns in the maps. The band contrast (BC) is extracted from the Kikuchi pattern analysis and represents the contrast of the Kikuchi bands (the higher, the better the Kikuchi pattern is). The mean angular deviation (MAD) is obtained from Hough transform of Kikuchi patterns and characterizes the misorientation between the fitted solution and measured band orientations (the lower, the better the solution is). Tab. 2 indicates that the best Kikuchi patterns, on both ferrite and cementite, were obtained using ionic polishing.

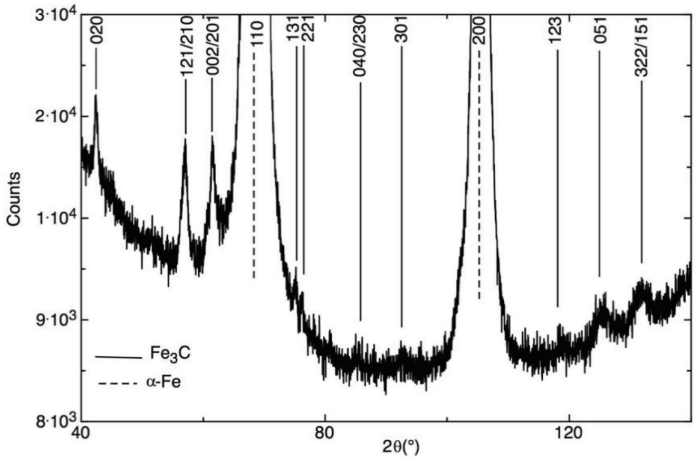

Fig. 3: X-ray diffraction spectrum of a nitrided 33CrMoV12-9 steel at 50 µm below the surface. Relative intensity of ferrite and cementite diffraction peaks.

Tab. 2: Quality of surface finishing preparations using several quality criteria (IR: indexing rate quality, BC: band contrast, MAD: mean angular deviation) of Kikuchi patterns for ferrite and cementite.

		Surface finishing preparation				
		Vibratory		**Ionic**		**Electrochemical**
Criterion	**Phase**	Aver.	Best	Aver.	Best	
IR	α-Fe	8.3	11.5	41.8	52.5	27.3
	Fe_3C	5.0	12.7	14.9	25.4	10.6
BC	α-Fe	65.0	105.0	80.1	91.9	73.7
	Fe_3C	67.0	102.0	63.7	68.0	50.6
MAD	α-Fe	0.75	0.67	0.66	0.59	0.70
	Fe_3C	0.84	0.77	0.83	0.77	0.91

EBSD analysis. Fig. 4 gives several maps from EBSD analyses of grain boundary cementite clusters and ferrite (Fig. 4a). The BC map (Fig. 4b) indicates polycrystalline cementite with a mean grain size around 0.73 ± 0.4 µm. The distribution of the grain size is given in Fig. 4f. The grain size of tempered martensite is close to 10 µm. Fig. 4c and Fig. 4e give the local misorientation between pixels and grains respectively. These qualitative criteria indicate that cementite is more strained than ferrite. The Euler angles map (Fig. 4d) and inverse pole figures (IPF) (Fig. 4g to 4i) give the orientations of cementite and ferrite grains.

Materials Research Proceedings **2** (2016) 133-144 doi: http://dx.doi.org/10.21741/9781945291173-24

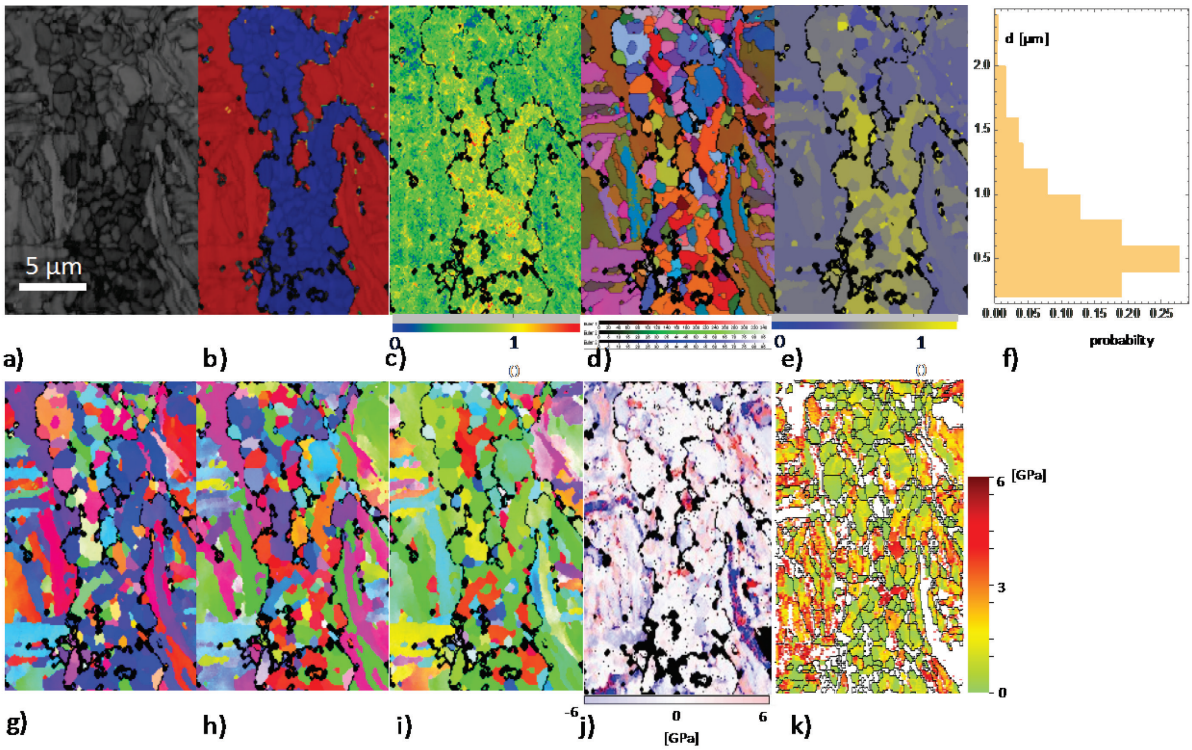

Fig. 4: Maps from EBSD analysis of grain boundary cementite clusters and ferrite (same scale on every map): a) band contrast, b) phases: red = α-Fe, blue = cementite, c) mean average disorientation between pixels d) Euler angles, e) mean average disorientation between grains, f) Fe_3C grain size distribution, g) IPFx, h) IPFy, i) IPFz, j) hydrostatic pressure, k) von Mises stress.

Texture. The EBSD Euler angles map indicates a local orientation of cementite at grain boundaries. Fig. 5a shows the inverse pole figures along X, Y and Z axes from EBSD analysis where the <101> direction remains perpendicular to the surface. The local anisotropy of cementite can be linked to the local ferrite grains anisotropy and the Bagaryatskii orientation relationship: $(100)_{Fe_3C} \parallel (0\bar{1}1)_\alpha, (010)_{Fe_3C} \parallel (0\bar{1}\bar{1})_\alpha, (001)_{Fe_3C} \parallel (211)_\alpha$ [17]. Because of a bigger gage volume and un-textured ferrite matrix, no texture is observed for cementite using X-ray diffraction according to the average contribution of the local textured cementite at grain boundaries (Fig. 5b). Consequently, XEC of cementite were calculated assuming an isotropic behaviour (as the ferrite phase).

Residual stresses. X-ray residual stress analyses were performed using ½S_({211})=5.83 ⟦10⟧^(-6) MPa^(-1) and ½S_({051})=6.22 10-6 MPa-1 for ⊣Fe and Fe3C respectively, according to calculations from single crystal elastic constants and the Kröner-Eshelby invariant method. Diffraction peaks were fitted using a pseudo-Voigt function and linear background. Residual stresses of both phases were considered as axisymmetric, so that stress analysis was performed in one direction [1]. It follows that compressive stresses of ⟦(σ⟧_xx^(α-Fe)-σ_zz^(α-Fe))=-1325±1 MPa without shear stresses and ⟦(σ⟧_xx^(Fe_3 C)-σ_zz^(Fe_3 C))=-619±92 MPa without significant shear stress were calculated for ferrite and cementite respectively. The local residual stress states from EBSD analysis in tempered martensite and cementite are given in Fig. 4j for the hydrostatic pressure and Fig. 4k for von Mises stresses. The cross-correlation method globally gives high stresses in absolute value (up to 6 GPa). The quality of the Kikuchi patterns was found very low generating non negligible correlation errors. The local (inside a selected orientation) stresses in tempered martensite appear higher than in cementite, that is in agreement with X-ray diffraction

measurements. Stress heterogeneities seem to be more important in ferrite due to the native microstructure (martensite laths).

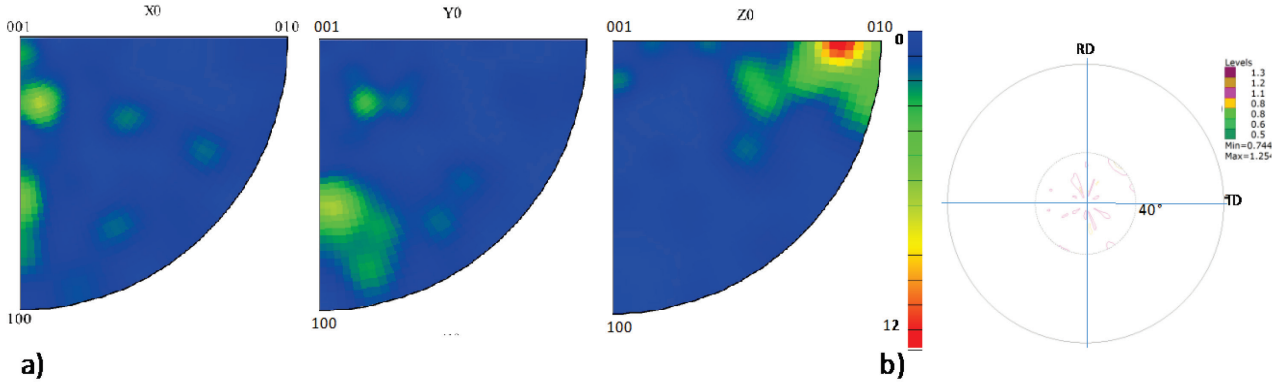

Fig. 5: Cementite texture analysis: a) IPF at the scale of grain boundaries from EBSD analysis, b) pole figure at the macroscopic scale using {121}/{210} diffracting planes (X-ray diffraction).

Conclusion

Residual stress analyses were performed in a nitrided layer using a local approach based on EBSD analysis and a pseudo-macroscopic approach based on X-ray diffraction both in the ferrite matrix and cementite at grain boundaries. Studied surface must be very well prepared using an optimized ionic surface polishing method for good quality EBSD analysis. Pseudo-macro-stresses were found compressive in both ferrite and cementite and the level of stress in cementite was twice less than in tempered martensite. Local stress analysis by EBSD is in agreements and shows strong mechanical heterogeneities between grains.

References

[1] L. Barrallier, Classical Nitriding of Heat Treatable Steel, in E.J. Mittemejier, M.A.J. Somers (Eds.), Thermochemical Surface Engineering of Steels, Elsevier Ed., 2014, pp. 392-410.

[2] D. Pye, Practical nitriding and ferritic nitrocarburizing, ASM International, 2003.

[3] L. Barrallier, PhD thesis, Arts et Métiers ParisTech, 1992.

[4] J.N. Locquet, PhD thesis, Arts et Métiers ParisTech, 1998.

[5] G. Fallot, PhD thesis, Arts et Métiers ParisTech, 2015.

[6] M.A. Terres, S.B. Mohamed, H. Sidhom, Int. J. of Fatigue, 32 (2010) 1795-1804.

[7] S. Jégou, PhD thesis, Arts et Métiers ParisTech, 2009.

[8] C. Mansilla, V. Ocelík, J.T.M. de Hosson, Mat. Sc. and Eng.: A, 636 (2015) 476-483. http://dx.doi.org/10.1016/j.msea.2015.04.023

[9] V. Goret, PhD thesis, Arts et Métiers ParisTech, 2006.

[10] M. Chaussumier, PhD thesis, Arts et Métiers ParisTech, 2000.

[11] C.C. Jiang, S. Srinivasan, A. Caro, S. Maloy, Journal of Applied Physics, 103 (2008).

[12] C. Maurice, R. Fortunier, Journal of Microscopy, 230 (2008) 520-529. http://dx.doi.org/10.1111/j.1365-2818.2008.02045.x

[13] A. Wilkinson, G. Meaden, D. Dingley, Ultramicroscopy, 1106 (2005) 307-313.

[14] A. Wilkinson, T. Britton, Materialstoday, 15, n°19 (2012).

[15] T. Britton, A. Wilkinson, Ultramicroscopy, 111, (2011) 1395-1404. http://dx.doi.org/10.1016/j.ultramic.2011.05.007

[16] L. Lutterotti, S. Matthies, H. Wenk, A. Schultz, J.J. Richardson, J. Appl. Phys., 81 (1997) 594-600. http://dx.doi.org/10.1063/1.364220

[17] Y. A. Bagaryatskii, Dokl. Akad. Nauk. SSSR, 73 (1950) 1161–1164.